RSC Advances

ROYAL SOCIETY OF CHEMISTRY

www.rsc.org/advances

The effect of peripheral substituents attached to the phthalocyanines on the third order nonlinear optical properties of graphene oxide–zinc (II) phthalocyanine hybrids

Zhao Wang,[a] Chunying He,*[a] Weina Song,[ab], Yachen Gao,[a] Zhimin Chen,[a] Yongli Dong,[ab] Cheng Zhao,[a] Zongle Li,[a] Yiqun Wu[a]

[a] *Key Laboratory of Functional Inorganic Material Chemistry, Ministry of Education, School of Chemistry and Materials Science, Heilongjiang University, Harbin 150080, PR China*

[b] *College of Environmental and Chemical Engineering, Heilongjiang University of Science and Technology, Harbin 150022, PR China*

Abstract

Two kinds of graphene oxide–zinc phthalocyanine (GO–ZnPc) hybrid materials have been prepared by the covalent functionalization method. The morphologies and structures of the two kinds of GO–ZnPc hybrids are characterized by a series of methods，such as scanning electron microscopy, atomic force microscopy, x-ray photoelectron spectroscopy, fourier transform infrared, ultraviolet-visible absorption and fluorescence spectroscopy. From fluorescence spectra, two kinds of GO–ZnPc hybrids display strong fluorescence quenching by the photo-induced electron transfer (PET) process from ZnPc moieties to the GO. Energy diagrams show that the PET process from ZnPc molecules to GO nanosheet exists. The third order nonlinear optical (NLO) properties of GO–ZnPc hybrids are investigated by the Z-scan technique at 532 nm with 4 ns laser pulses. The nonlinear absorption coefficient β value of GO-ZnPc$(DG)_4$ is larger than that of GO-ZnPc$(TD)_4$ because GO-ZnPc$(DG)_4$ possesses the peripheral substituents with the stronger electron-donating effect compared to GO-ZnPc$(TD)_4$.

* Corresponding author: Fax: +86 451 8667 3647

E-mail address: chunyinghe_hlju@163.com (C. He)

Introduction

Electro-optical sensors and eyes are easily injured by all kinds of strong light. A laser beam whose focused laser intensity is 350 times as great as sun can damage delicate optical instruments and human eyes. For this reason, nonlinear optical materials which act as optical-limiting materials and reverse saturable absorbers have been investigated by researcher so as to modulate the input light intensity.[1-5] In the past decade, significant research have been focused to find or synthesize large optical nonlinearities and fast nonlinear optical (NLO) response materials.[6-9] Recently, the carbon-based materials such as fullerenes, carbon nanotubes, graphene and carbon analogues exhibit excellent nonlinear optical (NLO) properties.[10-11] Graphene, a two dimensional (2D) monolayer which is an atom-thick sheet of sp^2-bonded carbon atoms arranged in a honeycomb lattice exhibits the special electrical and optical properties.[12] Thus, graphene oxide (GO) is a key functionalized analogue of graphene which captures interest for its physical properties.[13] Owing to its special structure, some characteristics of graphene is induced by the presence of pristine graphitic nanoislands, in which small sp^2 carbon nanoislands are isolated by the sp^3 matrix.[14] So the electrical, optical, and chemical properties of GO can be tunned by the degree of oxidation of GO.[15] In the last few years, the poor solubility of GO comes as the first obstacle for their optical applications. Therefore, formation of covalent bonds with soluble molecules to modify graphene materials in water or organic solvents was reported. As we kown, the π-conjugated organic molecules display stong reverse saturable absorption (RSA) because of their strong multiphoton absorption or excited state absorption. To our surprise, introduction of π-conjugated organic molecules such as porphyrins, phthalocyanines, and other large aromatic molecules to GO sheets can improve the optical limiting performance and enhance the NLO parameters.[15-16]

In previous work, our group researches on the solubility and enhancement of the third order NLO properties of GO based hybrids were reported.[17] RGO–ZnPc hybrid and GO–ZnPc [3-(2-[2-(2-hydroxyethoxy) ethoxy]ethoxy) phthalocyanine] were prepared and their third order nonlinear optical properties were studied using

532 nm, 4 ns laser pulses. RGO–ZnPc exhibited much larger NLO properties and OL performance than those of individual GO, ZnPc and the GO–ZnPc hybrid, ascribed to a combination of different NLO absorption behaviors. Subsequently, the relations between the NLO performance of RGO–MPc (M=Cu, Pb, Zn) hybrids and the molecular structure of phthalocyanines (alteration of central metal inserted in phthalocyanines) was investigated.[18] In this paper, two kinds of ZnPc [1,8,15,22-tera-(3-(5-hydroxyl)pentyloxy) phthalocyanine zinc ZnPc(TD)$_4$] and [1,8,15,22-tera-(3-[2-(2-hydroxyl)ethoxy]ethoxy) phthalocyanine zinc ZnPc(DG)$_4$] were synthesized and their GO-ZnPc hybrids prepared by covalent functionalization method. The two kinds of GO-ZnPc hybrids are characterized using a series of methods, and the NLO properties are studied using the Z-scan technique with 532nm, 4 ns laser pulses. The research results show that their nonlinear optical properties are affected by the structure of the peripheral substituents of phthalocyanines, and that stronger electron-donating group of the peripheral substituents can enhance NLO absorption effect of the GO-ZnPc hybrids.

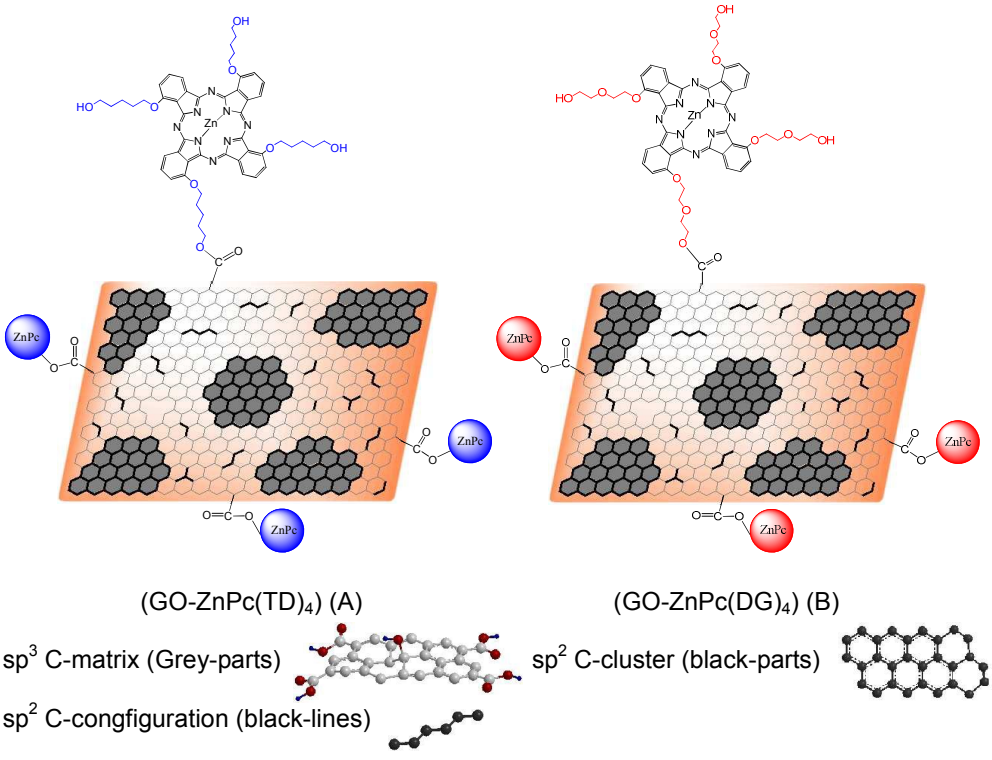

Fig.1 The synthesis scheme of GO-ZnPc(TD)$_4$ (A) and GO-ZnPc(DG)$_4$ (B).

Experimental section

Synthesis of $ZnPc(TD)_4$

1,8,15,22-tera-(3-(5-hydroxyl)pentyloxy) phthalocyanine zinc phthalocyanine zinc ($ZnPc(TD)_4$) was synthesized from 3-(5-hydroxyl)pentyloxy phthalonitrile which was similar to the synthetic route of 1,8,15,22-tetra-(2-hydroxyethyleneoxy) phthalocyanine zinc(II).[19] The 3-(5-hydroxyl) pentyloxy phthalonitrile (0.6 mmol), 1,8-diazabicyclo[5.4.0]undec-7-ene (DBU) (0.4 mL), anhydrous $Zn(OAc)_2$ (0.03 mmol) and 1-hexanol (25 mL) were mixed and refluxed for 18 h under nitrogen atmosphere. The reaction product was extracted with a water-chloroform (1:1) mixture into the chloroform phase. The organic layer evaporated to dryness to obtain the dark-green product. Then, the product was purified by column chromatography (silica gel, dichloromethane–ethanol mixture (3:1) as eluent). $ZnPc(TD)_4$ Yield: 0.119 g (80.4%). $C_{52}H_{56}N_8O_8Zn$ ^1H NMR (DMSO-d_6) δ 9.01-7.76 (bd, 12H, aromatics) 5.08–3.47 (m, 40H, CH_2), 4.71 (s, 4H, O–H). Elemental analysis found (calcd): C 67.76% (67.14%); H 6.03% (5.98%); N 12.23% (12.54%). IR [(KBr) ν_{max} (cm^{-1})]: 3305 (O-H), 2932 (C-H), 1438 (C=N). UV-Vis (DMSO): λ_{abs}= 706nm, 320nm. MALDI-TOF-MS found (calcd): 985.283 (984.85).

Synthesis of $ZnPc(DG)_4$

1,8,15,22-tera-(3-[2-(2-hydroxyl)ethoxy]ethoxy) phthalocyanine zinc ($ZnPc(DG)_4$) was synthesized from 3-[2-(2-hydroxyl)ethoxy]ethoxy phthalonitrile. The 1,8,15,22-tera-(3-[2-(2-hydroxyl)ethoxy]ethoxy) phthalocyanine zinc ($ZnPc(DG)_4$) was prepared based on the synthetic route of the 1,8,15,22-tetra-(3-(2-{2-[2-(2hydroxyethoxy)-ethoxy]ethoxy}ethoxy) phthalocyanine zinc(II).[19] 3-[2-(2-hydroxyl) ethoxy] ethoxy phthalonitrile (0.8 mmol), anhydrous $Zn(OAc)_2$ (0.05 mmol) and 1,8-diazabicyclo[5.4.0]undec-7-ene (DBU) (0.5 mL) were added into the 1-hexanol (20 mL). The mixture was stirred and refluxed for 24 h under nitrogen atmosphere, and the reaction mixture was diluted with dichloromethane (15 mL). The precipitated product was obtained from dichloromethane and purified by column chromatography (silica gel,

dichloromethane–ethanol mixture (5: 1) as eluent). $ZnPc(DG)_4$ Yield: 0.163 g (82.2%). $C_{48}H_{48}N_8O_{12}Zn$ ^1H NMR (DMSO-d_6) δ 9.09-7.31 (bd, 12H, aromatics) 5.19–3.44 (m, 32H, CH_2), 4.91 (s, 4H, O–H). Elemental analysis found (calcd): C 61.76% (62.06%); H 5.17% (5.21%); N 12.08% (12.06%). IR [(KBr) ν_{max} (cm^{-1})]: 3300 (O-H), 2930 (C-H), 1436 (C=N). UV-Vis (DMSO): λ_{abs}= 702nm, 324nm. MALDI-TOF-MS found (calcd): 992.459 (992.27).

Synthesis of GO

Graphene oxide (GO) was synthesized according to a modified Hummers method.[20] The graphite (4 g) was added in the mixture which contains 98% H_2SO_4 (40 mL), $K_2S_2O_8$ (6 g) and P_2O_5 (4 g). The mixture was stirring vigorously at 70 □ for 5 h. Then, the mixture was diluted with distilled water and filtered. The mixture was diluted with distilled water and filtered until the pH value of the rinse water pH is about 7. The preoxidized graphite was dried in a vacuum for 18 h. Furthermore, it was added into the mixed solution including 98% H_2SO_4 (80 mL), $NaNO_3$ (2 g) and $KMnO_4$ (10 g), and then the mixture was stirred vigorously. The stirring was sustained for 2 h at 0 □ and 2 h at 35 □. And distilled water (100 mL) was added and stirred 15 min. Finally, the solution was poured into de-ionized water, and a sufficient amount of H_2O_2 was added to destroy the excess permanganate. The mixture was filtered and washed with HCl (0.5 mol/L).The obtained purified GO was dried in vacuum at 20 □ for 32 h.

Synthesis of GO-ZnPc

Based on the covalent linkage of ZnPc to GO on the basis of ester groups,[17] two kinds of GO–ZnPc hybrids were synthesized in DMF solution. GO (50 mg) was dispersed in DMF (35 mL) by sonicated (400 w) for 40 min. Then, DCC (35 mg) was added into DMF solution of GO in order to activate the carboxyl groups at the edge of GO. The active reaction was stirred for 0.5 h. Subsequently, another DMF solution of $ZnPc(TD)_4$ or $ZnPc(DG)_4$ was added into the active reaction and was stirring for 5 days at room temprerature. Finally, the solid product was filtered by DMF and washed in DMF solution until the filtrate was colorless and transparent by ultrasonic-treatment in order to remove excess unreacted ZnPc or adsorbed ZnPc on

the GO sheets. And the product was dried at the vaccum at 40 □.

Characterization

The micrographs of Scanning electron microscope (SEM) were obtained with a HELIOS NANOLAB 600i instrument (FEI company). The samples which were used for Atomic force microscopy (AFM) were prepared by drop-casting on a silicon cantilever. The images of AFM were obtained by Digital Instruments Nanoscope IIIA. The X-ray photoelectron spectroscopy (XPS) was documented by Thermo ESCALAB 250 spectrometer with a monochromatic Al Ka X-ray as source (15 kV, 150 W). The C (1s) binding energy of carbon were taken to be 284.6 eV. Fourier transform infrared (FT-IR) spectra were acquired by a Perkin Elmer instruments Spectrum One FT-IR spectrometer (KBr disks). Ultraviolet-visible (UV-vis) spectra of samples were recorded by the Jena SPECORD S600 spectrophotometer with a quartz cell of 10mm path length. The Fluorescence spectra were performed with the Edinburgh instruments FLS920, and the excitation wavelength is 635 nm. The Electrochemical data was obtained by computer-controlled CHI 660D electrochemical workstation (CH Instrument, Shanghai, China) and was performed in 0.1 mol TBAP at room temperature. The conventional three-electrode system was used including a modified glassy carbon electrode, a platinum foil, and a silver chloride electrode.

Nonlinear optical measurement

The second harmonic of a Q-switched Nd: YAG laser (532 nm, 4 ns) was adopted as the laser source in the Z-scan experiments. The laser beam was adapted by an inverted telescope system which includes fluence attenuator and a Glan-Taylor prism. Then beam was focused by an f/100 mm convex lens (Zolix OLB50-100, Φ50, f 100) to a beam waist radius ω_0 of 50 mm. The laser beam was divided with a beam splitter because samples were loaded into the 2 mm quartz cell: the reflected beam worked as an open-aperture signal and the transmitted one which passed through a small hole (s = 0.10) worked as a close-aperture signal. The laser pulses were measued per 850 ms by energy detectors (PE9-ROHS energy probes, OPHIR Laser Measurement Group). The computer collected and analyzed the data from the energy detectors with the Zolix SC300-2A Motion Controller. The nonlinear absorption

coefficient β of the samples was determined by using the intensity variation equation and adopting an intensity-dependent absorption coefficient.[17]

Result and discussion

Morphological analysis

The morphologies of two kinds of GO-ZnPc hybrids are obtained with scanning electron microscope (SEM), and atomic force microscopy (AFM). The SEM images of the GO-ZnPc(TD)$_4$ hybrid and the GO-ZnPc(DG)$_4$ hybrid are shown in Fig.2(A) and Fig.2(C), both of which demonstrate the characteristics of turbostratic stacked flakes of graphene.[21-22] And the AFM images of GO-ZnPc(TD)$_4$ hybrid and the GO-ZnPc(DG)$_4$ hybrid are displayed in Fig.2(B) and Fig.2(D), exhibiting that the thickness of flake are ca. 3.8 nm and ca. 3.0 nm. The result indicates that the two kinds of GO-ZnPc hybrids can well maintain the structural features of few-layer graphene.

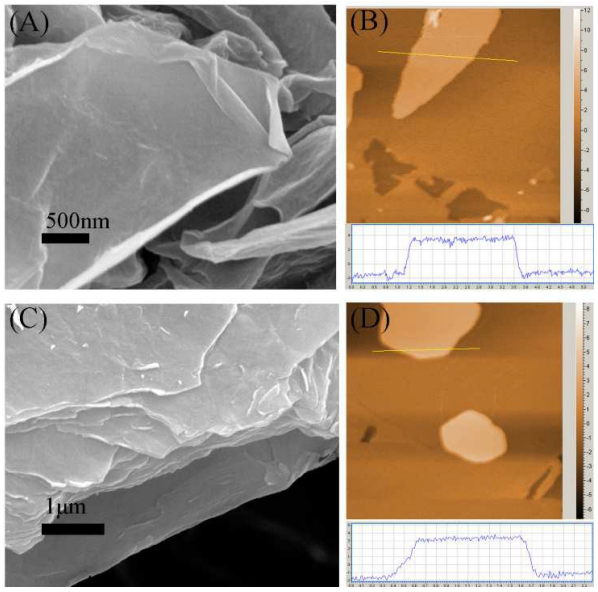

Fig.2 SEM images (GO-ZnPc(TD)$_4$ (A) and GO-ZnPc(DG)$_4$ (C)) and AFM images (GO-ZnPc(TD)$_4$ (B) and GO-ZnPc(DG)$_4$ (D))

FT-IR spectra

The FT-IR spectra are essential and useful method to testify covalent bonds of ZnPc moieties to GO. The FT-IR spectra of GO, GO-ZnPc(DG)$_4$, ZnPc(DG)$_4$, GO-ZnPc(TD)$_4$ and ZnPc(TD)$_4$ are shown in the Fig.3. The main characteristic

absorption peaks of GO are located at 1731 cm^{-1} ($\nu_{C=O}$) and 1415 cm^{-1} (δ_{O-H}) from carbonyl and carboxyl groups, 3416 cm^{-1} (ν_{O-H}) and 1046 cm^{-1} (ν_{C-O}) from hydroxyl groups, 1633 cm^{-1} ($\nu_{C=C}$) orginated from graphitic sheet and 1222 cm^{-1} (ν_{C-OH}) from epoxy/ether groups.[23] The characteristic absorption peaks of $ZnPc(TD)_4$ are located at at 3305 cm^{-1} (ν_{O-H}) and 1267 cm^{-1} (δ_{O-H}), at 2928 cm^{-1} (ν_{C-H}) and 1450 cm^{-1} (ν_{C-N}). And the characteristic absorption peaks of $ZnPc(DG)_4$ appears at 3307cm^{-1} (ν_{O-H}) and 1268 cm^{-1} (δ_{O-H}), at 2934 cm^{-1} (ν_{C-H}) and 1442 cm^{-1} (ν_{C-N}). Compared to ZnPcs, the new peak of ether group ($\nu_{C=O}$) for GO-$ZnPc(DG)_4$ is located at 1734 cm^{-1} and that for GO-$ZnPc(TD)_4$ is located at 1728 cm^{-1}. From the spectrum of GO-ZnPc hybrids, the ether group ($\nu_{C=O}$) and C-N bonds ($\nu_{C=N}$) are observed which suggests that the ZnPc molecules are introduced to the GO sheets.

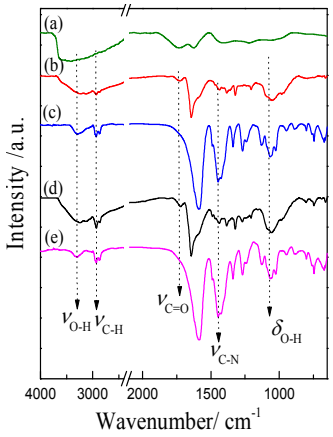

Fig.3 FT-IR spectra of GO (a), GO-$ZnPc(DG)_4$ (b), $ZnPc(DG)_4$ (c), GO-$ZnPc(TD)_4$ (d) and $ZnPc(TD)_4$ (e)

Raman spectra

The Raman spectra are good methods to analyze the GO-ZnPc hybrids, which display changes about the rates of sp^2 carbon (G band) and sp^3 carbon (D band) by introducing ZnPc moieties. The Raman spectra of GO, GO-$ZnPc(TD)_4$, GO-$ZnPc(DG)_4$ are shown in Fig.4. GO displays G band at 1587 cm^{-1} and obviously D band at 1361 cm^{-1}, which represents sp^2 carbon atoms domains and the vibrations of sp^3 carbon atoms, respectively.[24] Compared to GO, the G band of GO-$ZnPc(DG)_4$ appears at 1582 cm^{-1} and the G band of GO-$ZnPc(TD)_4$ appears at 1585 cm^{-1}. The 5 nm blue shift for GO-$ZnPc(DG)_4$ and 2 nm blue shift for GO-$ZnPc(TD)_4$ with respect

to G band of GO sheet suggest that electron transfer from the donor molecules (ZnPc) to the acceptor molecules (GO).[25-26] And, the G band of GO-ZnPc(DG)$_4$ exhibit blue shift of 3 cm^{-1} compared with that of GO-ZnPc(TD)$_4$, indicating that the peripheral substituents of ZnPc(DG)$_4$ have stronger ability to donate electron.[27-28]

The I_D/I_G ratio value of GO GO-ZnPc(DG)$_4$ and GO-ZnPc(TD)$_4$ powder is 0.84, 0.74 and 0.75, respectively. After the high efficient covalent linkage of the ZnPc to GO, the I_D/I_G ratio value of GO-ZnPc(DG)$_4$ or GO-ZnPc(TD)$_4$ decreases relative to that of GO because the ZnPc molecules grafted onto GO sheets contain a large amount of sp^2 aromatic carbon atoms. Additionally, the I_D/I_G ratio value of GO-ZnPc(TD)$_4$ have slightly larger than that of GO-ZnPc(DG)$_4$ because the peripheral substituents of ZnPc(TD)$_4$ has more sp^3 C than that of ZnPc(DG)$_4$.

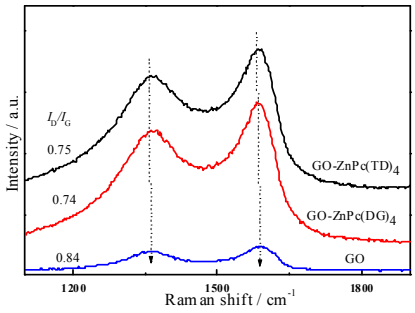

Fig.4 Raman spectra of GO, GO-ZnPc(DG)$_4$ and GO-ZnPc(TD)$_4$.

X-ray photoelectron spectroscopy

The elemental speciation of the GO–ZnPc hybrids has been investigated by XPS, which provided vital and significant information for the covalent attachment of the ZnPc molecules onto the edge of GO. The XPS spectra of GO, GO–ZnPc(TD)$_4$ and GO–ZnPc(DG)$_4$ are shown in Fig.5(A). Obviously, only two main characteristic peaks corresponding to the C 1s and O 1s species can be observed in the spectra of GO. After the covalent functionalization, four additional peaks of Zn 2p$_{1/2}$, Zn 2p$_{3/2}$, Zn Auger and N 1s in both the two kinds of GO–ZnPc hybrid are obviously observed at 1040.4 eV, 1018.9 eV, 494.8 eV and 396.3 eV, indicating that ZnPc molecules are introduced into GO nanosheets. Furthermore, the C/O mole ratios of GO (2.3), GO-ZnPc(DG)$_4$ (3.2) and GO-ZnPc(TD)$_4$ (3.6) are also obtained on the basis of XPS results. The relative peak intensity ratios of C 1s to O 1s for the GO-ZnPc(DG)$_4$ and

GO-ZnPc(TD)$_4$ hybrids increase with respect to that of GO. The increasement of mole ratios for the hybrids can be ascribed to the introduced ZnPcs because the amount of the C is obviously higher than that of the O in ZnPcs, especially for ZnPc(TD)$_4$ material. The C1s spectra of GO, GO-ZnPc(DG)$_4$ and GO-ZnPc(TD)$_4$ are further analyzed from Fig.5(B). In the C1s XPS spectrum, GO can be fitted into four peaks[29] which contains C-C (sp^2 carbon) at 284.9 eV, C-O at 286.2 eV, C=O at 287.1 eV and C(O)O at 288.0 eV, suggesting a degree of oxidation for the GO nanosheets. But, both the two C1s XPS spectra of GO-ZnPc(DG)$_4$ and GO-ZnPc(TD)$_4$ contains four peaks which are C-C, C-O, C=O, and C(O)O, respectively, orginanting from GO and one additional C-N species from the Pcs macrocycle appears at 285.7 eV.[28-29]

The peak area ratios of carbon-containing bonds to total area are also calculated on the basis of XPS results, as shown in Table 1. The peak area ratio of C-O bonds in GO–ZnPc hybrids is smaller than that of GO because ZnPc molecules possess few content of C-O bonds.

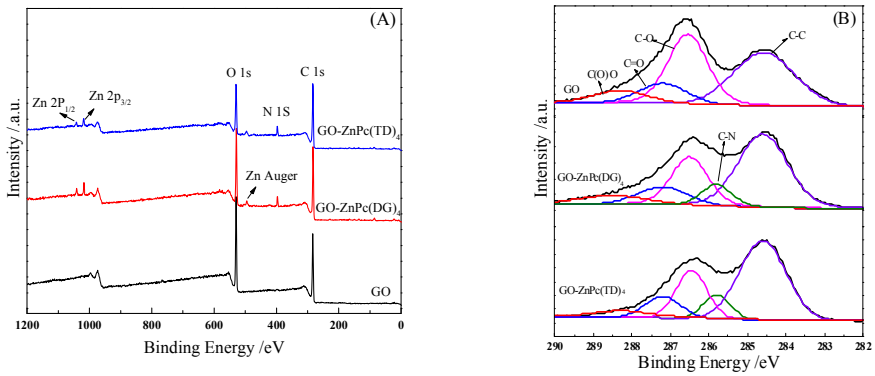

Fig.5 (A) XPS spectra of GO, GO-ZnPc(DG)$_4$, and GO-ZnPc(TD)$_4$ and (B) C1s XPS spectra of GO, GO-ZnPc(DG)$_4$, and GO-ZnPc(TD)$_4$

Table 1 The peak area (A) ratios of carbon-containing bonds to total area (A_T) according to the XPS results

Sample	A_{C-C}/A_T(%)	A_{C-O}/A_T(%)	$A_{C=O}/A_T$(%)	$A_{C(O)O}/A_T$(%)	A_{C-N}/A_T(%)
GO	41.3	37.6	12	9	
GO-ZnPc(DG)$_4$	48.5	24.2	11.1	7.4	8.7
GO-ZnPc(TD)$_4$	51.7	20.7	10.4	8	9

UV-vis absorption spectra

The UV-vis absorption spectra of ZnPc(DG)$_4$ and ZnPc(TD)$_4$) in DMSO

solution (2×10^{-4} mol/L) are shown in Fig.6(A). Both the spectra of $ZnPc(TD)_4$ and $ZnPc(DG)_4$ display characteristic absorption of metal phthalocyanines (MPcs) with an intense S_0-S_1 transition band (Q-band) followed by a smaller shoulder and a weak broad Soret band around at 300–350 nm. As shown in Fig.6(A), $ZnPc(DG)_4$ exhibit three main absorption peaks, such as B band at 320nm in ultraviolet band, Q bands at 632 nm and 702 nm in visible region.[30] For $ZnPc(TD)_4$, 4 nm red shift of Q band occurred relative to that of $ZnPc(DG)_4$. The red shift of Q band for $ZnPc(TD)_4$ compared to $ZnPc(DG)_4$ is caused by the peripheral substituent because the two kinds of ZnPc possess the same central metal. More alkyl groups can overlap with the π-electron of the conjugation system and generate hyperconjugation,[31-34] which enhances electronic motion, decreases the energy gap from HOMO to LUMO and induces absorption to shift to long wavelength.[35-39] So, $ZnPc(TD)_4$ has more alkyl group to induce the red shift compared with that of $ZnPc(DG)_4$.

From Fig.6(B), the UV-Vis spectrum of GO in DMSO has two featured peaks around 260 nm due to $\pi-\pi^*$ transition of aromatic C=C bonds, and a broad shoulder between 295 and 303 nm ascribed to n-to-π^* transition of C=O bonds. The spectra of $ZnPc(TD)_4$ and $ZnPc(DG)_4$ hybrids measured in DMSO solution (0.13 mg/mL) display the characteristic Q band of ZnPc. The Q band peaks of GO-$ZnPc(DG)_4$ show 6 nm and 4 nm red shift in contrast with that of $ZnPc(DG)_4$ and $ZnPc(TD)_4$, respectively, steming from the electron transfer from the ZnPc to GO. It is observed that the red shift of the Q band for the GO-$ZnPc(DG)_4$ is larger than that of GO-$ZnPc(TD)_4$, indicating that the charge transfer from the $ZnPc(DG)_4$ to GO is stronger than that from the $ZnPc(TD)_4$ to GO.

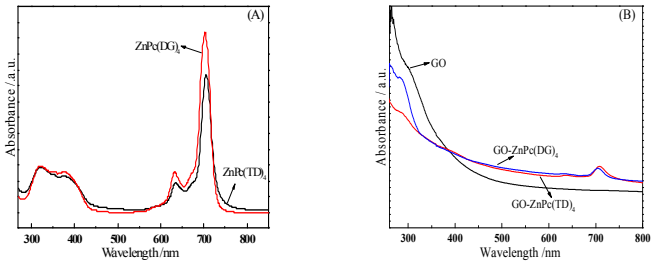

Fig.6 UV-vis absorption spectra of ZnPc (A) and GO–ZnPc hybrids (B).

Fluorescence spectroscopy

The fluorescence emission spectra of zinc (II) phthalocyanine complexes and their GO-ZnPc hybrids are given in Fig.7. Both concentrations of $ZnPc(TD)_4$ and $ZnPc(DG)_4$ are 1×10^{-5} mol/L, which are the same as that of standard unsubstituted-ZnPc. The weight fraction of phthalocyanines in $GO\text{-}ZnPc(TD)_4$ and $GO\text{-}ZnPc(DG)_4$ are determined from the atomic absorption spectrometry to be 19.88% and 19.45%, respectively. The concentrations of $GO\text{-}ZnPc(TD)_4$ and $GO\text{-}ZnPc(DG)_4$ for the experiments of Fluorescence spectroscopy are 0.068 mg/mL and 0.063 mg/mL, respectively, in which the amounts of both $ZnPc(TD)_4$ and $ZnPc(DG)_4$ are 1×10^{-5} mol/L. The maximum emission peaks of $ZnPc(DG)_4$ and $ZnPc(TD)_4$ are listed in Table 2, corresponding to the fluorescence of the S_1-S_0 transition.[40] The Stokes shift of $ZnPc(DG)_4$ is 12 nm, whereas $ZnPc(TD)_4$ is 7 nm. The fluorescence quantum yield (Φ_F) is calculated by the comparative method that unsubstituted-ZnPc (Φ_F = 0.20 in DMSO) is used as the standard. The Φ_F values of $ZnPc(TD)_4$ (0.06) are clearly smaller than $ZnPc(DG)_4$ (0.10) in the Table 2, resulting from the fact that the peripheral substituents of $ZnPc(DG)_4$ have stronger electron-donating effect than that of $ZnPc(TD)_4$. The peripheral substituents with the stronger electron-donating capacity could increase the electronic cloud density and enhance the fluorescence quantum yield of the phthalocyanine molecules. As shown in Fig.7((B)–(C)) and Table 2, the two kinds of GO–ZnPc hybrids exhibit weak emission intensity compared with the corresponding ZnPc molecules, and the fluoresccence quantum yield (Φ_F) of the former is much lower than that of the latter because of the strong electronic interaction between the GO and ZnPc moieties. ZnPc molecules have high performance as electron transporting antenna, and the graphene materials are the excellent acceptor of energy and electrons. Therefore, the fluorescence quenching of GO–ZnPc hybrids is induced by the photo-induced elecetron transfer (PET) from ZnPc to GO,[41] and possibility of PET process between ZnPc and GO will be analyzed in Thermodynamics of PET section.

The fluorescence quantum yield of $GO\text{-}ZnPc(DG)_4$ is 0.0045, decreased from 0.10 of $ZnPc(DG)_4$, and the difference value of fluorescence quantum yield between

the GO-ZnPc(DG)$_4$ hybrids and the ZnPc moiety is 0.0955. With the similar calculation methods, the same difference value of GO-ZnPc(TD)$_4$ is 0.0531. The PET efficiency between GO and ZnPc molecules depends on the capacity of electron transfer from ZnPc to GO. The efficient PET/ET process between GO and ZnPc especially depends on the difference value of fluorescence quantum yield between the GO-ZnPc(DG)$_4$ hybrids and the ZnPc moiety. Naturally, it is presumed that ZnPc(DG)$_4$ have stronger ability to donate electron compared to ZnPc(TD)$_4$ so as to induce GO-ZnPc(DG)$_4$ to possess stronger capacity of charge transfer. The S_1 excitation energies (Es) of GO-ZnPc hybrids are calculated from that of ZnPc(DG)$_4$ or ZnPc(TD)$_4$ because GO can not be excited. By using the absorption and emission spectra (Fig.8),[42] Es of GO-ZnPc hybrids can be obtained, namely 1.74 and 1.75 eV.

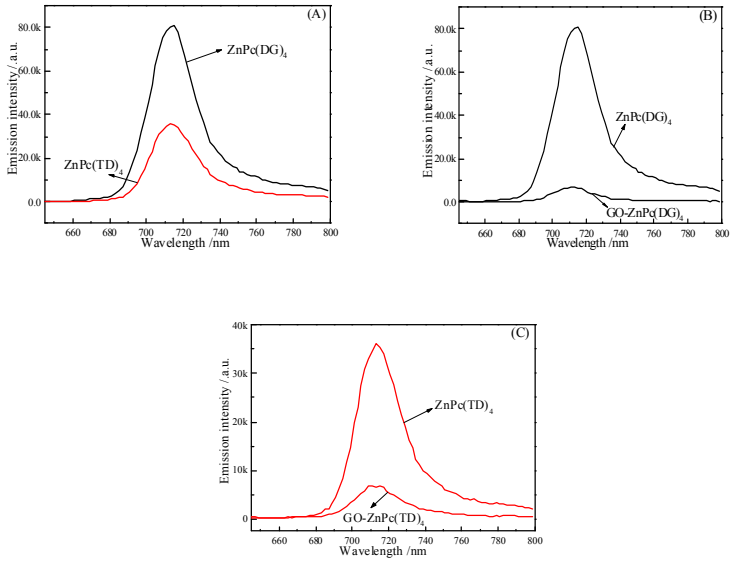

Fig.7 Steady state fluorescence spectra of ZnPc (A), ZnPc(DG)$_4$ and GO-ZnPc(DG)$_4$ (B), and ZnPc(TD)$_4$ and GO-ZnPc(TD)$_4$ (C).

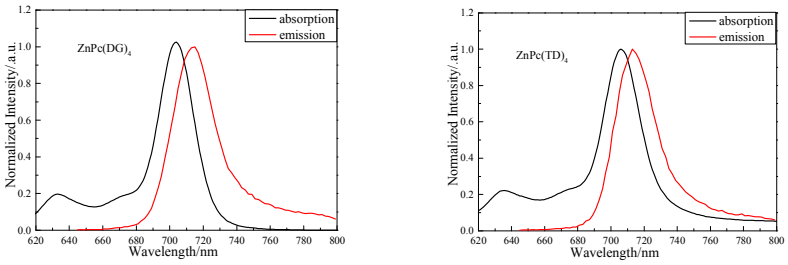

Fig.8 Normalized absorption and fluorescence (excitation at 635 nm) spectra of ZnPc(DG)$_4$

and $ZnPc(TD)_4$ in DMF.

Table 2 The absorption and emission spectra parameters (λ_{abs}, λ_{ex} and λ_{em}) and the fluorescence quantum yield (Φ_F) of ZnPc and GO–ZnPc hybrids

Sample	λ_{abs}/nm	λ_{ex}/nm	λ_{em}/nm	Φ_F
$ZnPc(DG)_4$	702	635	714	0.10
$ZnPc(TD)_4$	706	635	713	0.06
GO-$ZnPc(DG)_4$	708	635	710	0.0045
GO-$ZnPc(TD)_4$	710	635	712	0.0069

Thermodynamics of PET

Fig.9 gives the energy level model used in describe the interaction of light with a molecule compound in terms of electronic transitions in the material including the PET process of GO-ZnPc hybrids. Within a few femtoseconds, the ground state (S_0) of ZnPc moieties in the GO-ZnPc hybrids is excited to a higher vibronic level of the first singlet state (S_1) by a laser. Several competing processes can occur from here. Normally, these are further fluorescence from the first excited singlet state (S_1) to the ground state (S_0), or intersystem crossing from S_1 to the triplet state (T_1). Nonlinear absorption observed here is a consequence of T_1-T_2 absorption under the experiments with nanosecond pulse width. However, another process could happen from S_1 state to charge separated state (CSS state) by the photo-induced electron transfer (PET).

The redox properties of $ZnPc(DG)_4$ and $ZnPc(TD)_4$ are measured by cyclic voltammetry, and used to calculate the singlet level of the first excited state and triplet level of the first excited state. Then, above data is intergrated to get level model in order to discuss the possibility of the PET process from ZnPc moieties to GO in the two kinds of GO–ZnPc hybrids in Fig.8. The oxidation potential of $ZnPc(DG)_4$ and $ZnPc(TD)_4$ monomer in DMF is 0.63 V and 0.58 V, and the reduction potential of them is -0.43 V and -0.45 V, suggesting that two kinds of ZnPc could act not only as the good electron donor but also the electron acceptor. Different from a small molecule, GO nanosheet is a multiple electron acceptor, and the reduction potential of GO is in the region from -0.60 V to -0.85 V.[43-44]

The ground state electron transfer from ZnPc to GO nanosheet is forbidden because the free energy changes ΔG_{ET} are positive, where ΔG_{ET}= $E(Ox/Ox^{+})$-$E(Re/Re^{-})$-0.06, $E(Ox/Ox^{+})$ is the oxidation potential of a donor, $E(Re/Re^{-})$ represents the reduction potential of an acceptor. The ΔG_{ET} value are obtained to be in the range of $1.17eV \leqslant \Delta G_{ET(DG)} \leqslant 1.42eV$ and $1.14eV \leqslant \Delta G_{ET(TD)} \leqslant 1.39eV$. However, with light excitation of $ZnPc(DG)_4$ or $ZnPc(TD)_4$ to S_1, electron transfer to GO becomes thermodynamically favored, since the calculated ΔG_{PET} ($\Delta G_{PET} = \Delta G_{ET} - Es$) are negative values obtained by the following eqation: $\Delta G_{PET} = \Delta G_{ET}$-Es ($ZnPc(DG)_4$ or $ZnPc(TD)_4$). These results predict that $[ZnPc(DG)_4]^{+}$ or $[ZnPc(TD)_4]^{+}$ and GO^{-} are formed upon photoexcitation of ZnPc ($ZnPc(DG)_4$ or $ZnPc(TD)_4$) molecules, and PET process from ZnPc molecules to GO nanosheet exists.

$$S_0(ZnPc(DG)_4) \xrightarrow{h\nu} S_1(ZnPc(DG)_4), \quad Es = 1.75\ eV \qquad (1)$$

$$S_1(ZnPc(DG)_4) + GO \rightarrow (ZnPc(DG)_4)^{+} + GO^{-} \quad -0.6eV \leqslant \Delta G_{PET} \leqslant -0.33eV$$

$$S_0(ZnPc(TD)_4) \xrightarrow{h\nu} S_1(ZnPc(TD)_4), \quad Es = 1.74\ eV \qquad (2)$$

$$S_1(ZnPc(TD)_4) + GO \rightarrow (ZnPc(TD)_4)^{+} + GO^{-} \quad -0.6eV \leqslant \Delta G_{PET} \leqslant -0.35eV$$

The emission peak wavelength of phosphorescence of unsbstituted ZnPc[45] is adopted to calculate the T_1 state energy of $ZnPc(DG)_4$ or $ZnPc(TD)_4$,[45] since the maxima of phosphorescence emission spectra are not altered remarkably by substituent from 1.1 eV of unsbstituted ZnPc and are mainly affected by π-conjugated system and central metal.[45] The T_1 state formation could originate from two paths: one is from S_1 state to charge separated state (CSS state) by the photo-induced electron transfer (PET) and the other is from S_1 state to triplet excited state (T_1 state) by the intersystem crossing (ISC). At last, ZnPc-^{3}GO in the T_1 state are transmitted to the ground state with the radiative transition. The energy level models exhibit that the PET process induces the ZnPc moieties in S_1 state to transmite to the CSS state. This T_1 formation process and subsequent the T_1-T_2 absorption are made possible because

the CSS has a higher energy ($1.17eV \leqslant \Delta G_{ET(DG)} \leqslant 1.42eV$ $1.14eV \leqslant \Delta G_{ET(TD)} \leqslant 1.39eV$) than that of ZnPc-^{3}GO (1.10eV), as shown in Fig.9.[44-45]

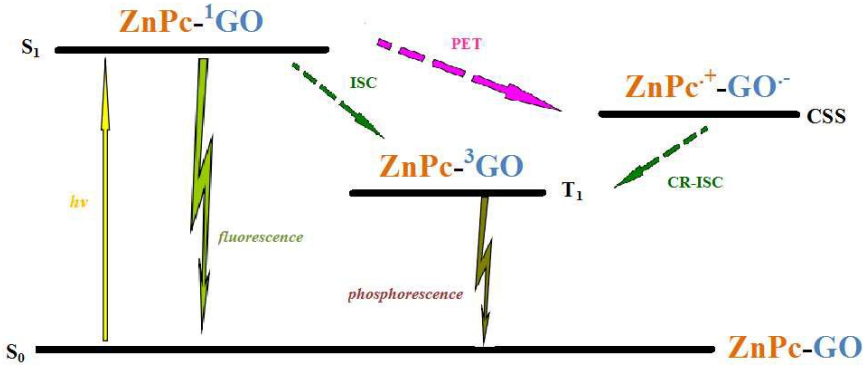

Fig.9 Level model show that the PET process of GO-ZnPc hybrids

The third order nonlinear optical properties

The third order NLO properties of GO, ZnPc and GO-ZnPc hybrids were measured by Z-scan technique with the imput intensity of 0.326 J/cm^2. The concentration of ZnPc(DG)$_4$ and ZnPc(TD)$_4$ in DMSO is 2×10^{-4} mol/L, and the samples of GO and GO-ZnPc hybrids are dispersed in DMSO a concentration of 0.13 mg/mL by ultrasonic treatment. The content of GO or ZnPc in GO-ZnPc hybrids is evidently smaller than that of pure GO or ZnPc, calculated by the weight fraction of phthalocyanines in GO-ZnPc hybrids. The curves of ZnPc(DG)$_4$ and ZnPc(TD)$_4$ exhibit the typical valley of RSA in Fig.10(A), resulting from the excited state absorption of ZnPc molecules. And the nonlinear absorption coefficient β value of different ZnPc molecules decreases in the order of ZnPc(DG)$_4$ (17 cm/GW) > ZnPc(TD)$_4$ (11.03 cm/GW) because ZnPc(DG)$_4$ possesses larger electron cloud density deduced from fluorescence analysis. The large electron cloud density of phthalocyanines can accelerate the intersystem crossing and increase the polarizability of the delocalized π conjugated systems to improve the third order NLO properties.

The normalized transmission curves of GO and GO-ZnPc hybrids in Fig.10(B) show two weak shoulder peaks along with a deep valley, indicating transformation of the NLO response from SA to RSA with the increase of the pump intensity.[46] It can be

easily seen that the two kinds of GO–ZnPc hybrids shows a much deeper valley than that of GO. The theoretically fitted β value of GO, GO-ZnPc(DG)$_4$ and GO-ZnPc(TD)$_4$ is 80 cm/GW, 360 cm/GW and 280 cm/GWs, respectively.[47] The reason why the two kinds of GO-ZnPc hybrids possess larger nonlinear absorption coefficient β value with respect to that of GO and the corresponding ZnPc is that unique atomic and electronic structure of GO and ZnPc molecules. Moreover, the PET/ET process between ZnPc and GO documented in fluorescence analysis may lead to a combination of NLO absorption arising from the GO and ZnPc moieties.[17-18] The significantly enhanced NLO properties of the two kinds of GO–ZnPc hybrids can be ascribed to the combination of different nonlinear absorption (NLA) mechanisms, including the two-photon absorption (TPA) originating from the sp^3 carbon domains of GO moiety, the excited state absorption (ESA) from small localized sp^2 configurations of GO moiety, saturable absorption (SA) from the sp^2 carbon clusters of GO moiety and the excited state absorption of ZnPc moiety based on the first triplet state.[17-18]

Furthermore，the nonlinear absorption coefficient β value of GO-ZnPc(DG)$_4$ is obviously larger than that of GO-ZnPc(TD)$_4$, which is in good agreement with the above mentioned order of β value as ZnPc(DG)$_4$ > ZnPc(TD)$_4$. Based on above analysis, the nonlinear optical absorption of GO-ZnPc hybrids mainly result from the the combination of different nonlinear absorption (NLA) originating from the GO moiety and ZnPc molecules, and PET/ET process between ZnPc moieties and GO. Therefore, the stronger nonlinear optical absorption effect of ZnPc molecules is, the larger β value of the GO-ZnPc hybrids is. In addition, the PET/ET process between ZnPc and GO described in fluorescence analysis may also devote to the NLO absorption by the fluorescence quenching and energy releasing. The possibility of the PET process between ZnPc and GO has been confirmed in the thermodynamics of PET section.[48] In the process of PET, ZnPc molecules act as electron donators, while GO nanosheet preserves as a good electron acceptor. The PET efficiency between GO and ZnPc molecules depends on the capacity of electron transfer from ZnPc to GO. In combination with the analysis of fluorescence spectra, the efficient PET/ET process

between GO and ZnPc especially depends on the difference value of fluorescence quantum yield between the GO-ZnPc$(DG)_4$ hybrids and the ZnPc moiety. The larger the difference value of fluorescence quantum yield between the GO-ZnPc hybrids and the ZnPc moiety is, the higher PET efficiency between ZnPc and GO is. This is because the PET process between ZnPc and GO must lead to the results of the fluorescence quenching and decreasing of the fluorescence quantum yield. The peripheral substituents of ZnPc$(DG)_4$ have stonger ability to donate electron and is much easier to transfer electron to GO than that of ZnPc$(TD)_4$. When GO-ZnPc$(DG)_4$ is excited by laser, it is easier for ZnPc$(DG)_4$ to transfer electron to GO and to exhibit the stronger nonlinear optical absorption effect in comparism with GO-ZnPc$(TD)_4$. The above results hint that the NLO absorption performance originates from not only the combination of ZnPc and GO but also the contribution of the efficient PET process. In summary, the peripheral substituents of ZnPc play important role in the photophysical and nonlinear optical properties of the GO–ZnPc hybrid materials. The transition from CSS to T_1 can increase the atomic population in T_1 state so as to improve the NLO properties.

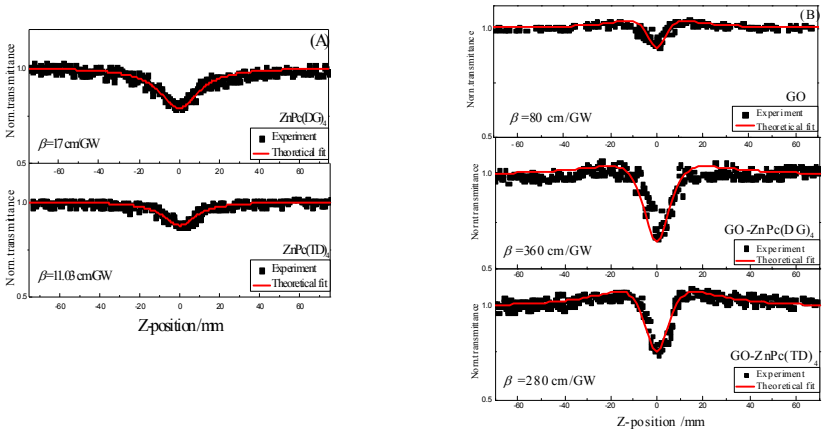

Fig.10- Open aperture Z-scan curves of the GO, ZnPc and GO–ZnPc hybrid materials

Conlusion

Two kinds of GO–ZnPc hybrid materials were prepared and characterized by FT-IR, XPS, Raman and UV-vis spectra, which provides information for the covalent attachment of the ZnPc moieties into GO nanosheet. The morphologies of GO-ZnPc hybrids are obtained by SEM, AFM, exhibiting the stacked graphene flakes of with

few layers. By using the fluorescence spectra and thermodynamics of PET, it proves that the PET process from ZnPc molecules to GO nanosheet exists and improves the formation of T_1 state. The third order NLO properties of the two kinds of GO–ZnPc hybrid materials were investigated using Z-scan technique, and the peripheral substitution function of phthalocyanine molecule in the two kinds of GO-ZnPc hybrids on the nonlinear absorption was investigated. The two kinds of GO–ZnPc hybrids showed stronger NLO absorption effect than that GO and the corresponding phthalocyanines, attributing to the combination of different NLO mechanism of ZnPc and GO moieties and the contribution of the PET process from ZnPc to GO. Furthermore, the nonlinear absorption coefficient β values of the two GO-ZnPc hybrids increase in order of GO-ZnPc$(DG)_4$ > GO-ZnPc$(TD)_4$ because the peripheral substituents of ZnPc$(DG)_4$ have stronger electron-donating effect than that of ZnPc$(TD)_4$. The stronger electron-donating of peripheral substituents can increase the electronic cloud density of delocalized π-conjugated system to improve NLO absorption effect. In a word, the GO-ZnPc$(DG)_4$ hybrid in which ZnPc$(DG)_4$ moieties possess the stronger electron-donating group is one kind of the most promising material for optical limiting, optical switching and solar energy conversion applications.

Acknowledgments

This work is supported by the National Natural Science Foundation of China (21203058, 51002046 and 61275117), Natural Science Foundation of Heilongjiang Province of China (B201308, F201112), Foundation of Educational Commission of Heilongjiang Province of China (12521399 and 12531579), Natural Science Foundation for the Returned Overseas Scholars of Heilongjiang Province (LC2012C02) and the Innovative Talents Program of Heilongjiang University of Science and Technology (Q20130202).

References

1. Y. Chen, M. Hanack and Y. Araki, *Chem*. *Soc*. *Rev*., 2005, 34, 517–29.

2. Y. Chen, Y. Lin, Y. Liu, J. Doyle, N. He and X. Zhuang, *J. Nanosci. Nanotechnol*., 2007, 7, 1268–83.
3. CW. Spangler, *J. Mater. Chem*., 1999, 9, 2013–20.
4. Y. Chen, Y. Lin and N. He, *SPIE. Newsroom*., 2007, doi: 10.1117/2.1200706.0750.
5. Y. Chen, M. E. EI-Khouly, J. J. Doyle, Y. Lin and Y. Liu, *Handbook of organic electronics and photonics*, 2008, 2, 151–81.
6. M. Feng, H. B. Zhan and Y. Chen, *Appl. Phys. Lett*., 2010, 96, 033107.
7. L. Polavarapu, N. Venkatram, W. Ji and Q. H. Xu, *ACS. Appl. Mater. Interfaces*., 2009, 11, 2298−2303.
8. J. Wang, Y. Hernandez, M. Lotya, J. N. Coleman and W. J. Blau, *Adv. Mater*., 2009, 21, 2430−2435.
9. M. Scalora, J. P. Dowling, C. M. Bowden and M. Bloemer, *Phys. Rev. Lett*., 1994, 73, 1368−1371.
10. L. Polavarapu, Q. H. Xu, M. S. Dhoni and W. Ji, *Appl. Phys.* Lett., 2008, 92, 263110.
11. Y. H. Lee, Y. Yan, L. L. Polavarapu and Q. H. Xu, *Appl. Phys. Lett*., 2009, 95, 023105.
12. A. K. Geim and K. S. Novoselov, *Nat. Mate*., 2007, 6, 183–191.
13. D. Chen, H. Feng and J. Li, *Chem. Rev*., 2012, 11, 6027−6053.
14. K. Erickson, R. Erni, Z. Lee, N. Alem, W. Gannett and A. Zettl, *Adv. Mater*., 2010, 22, 4467–72.
15. N. Liaros, P. Aloukos and A. Kolokithas-Ntoukas, *J. Phys. Chem. C*., 2013, 117, 6842−6850.
16. X. F. Jiang, L. Polavarapu and S. T. Neo, *J. Phys. Chem. Lett.*, 2012, 3, 785−790.
17. W. Song, C. He, W. Zhang, Y. Gao, Y. Yang, Y. Wu, Z. Chen,X. Li and Y. Dong, *Carbon*, 2014, 77, 1020–1030.
18. W. Song, C. He, W. Zhang, Y. Gao, Y. Yang, Y. Wu, Z. Chen, X. Li and Y. Dong, *Phys. Chem. Chem. Phys*., 2015, 17, 7149—7157.

19. S. Tuncel and F. Dumoulin, *Dalton. Trans*., 2011, 40, 4067–4079.
20. W. S. Hummers and R. E. Offeman, *J. Am. Chem. Soc*., 1958, 80, 1339.
21. M. Bala, N. Venkatramaiah, R. Venkatesan and D. Narayana Rao, *J. Mater. Chem*., 2012, 22, 3059–3068.
22. W. Li, F. Wang, S. Feng, J. Wang, Z. Sun, B. Li, Y. Li, J. Yang, A. A. Elzatahry, Y. Xia and D. Zhao, *J. Am. Chem. Soc*., 2013, 135, 18300–18303.
23. X. Zhang, Y. Huang, Y. Wang, Y. Ma, Z. Liu and Y. Chen, *Carbon*, 2009, 47, 334–337.
24. S. Stankovich, D. A. Dikin, R. D. Piner, Kohlhaas, K. A. Kleinhammes and Y. Jia, *Carbon*, 2007, 45, 1558–65.
25. B. Zhang, Y. Chen, G. Liu, L. Xu, J. Chen and C. Zhu, *J. Polym. Sci. Part A*: *Polym. Chem*., 2012, 50, 378–87.
26. C. Mattevi, G. Eda, S. Agnoli, S. Miller, K. A. Mkhoyan,O. Celik, D. Mastrogiovanni, G. Granozzi, E. Garfunkel and M. Chhowalla, *Adv. Funct. Mater*., 2009, 19, 2577–2583.
27. S. Wang, Q. Gan, Y. Zhang, S. Li, H. Xu and G. Yang, *Chem. Phys. Chem*., 2006, 7, 935–941.
28. N. Kobayashi, S. Nakajima, H. Ogata, T. Fukuda, *Chem. Eur. J*., 2004, 10, 6294−6312.
29. Y.-O. Yeung, R. C. W. Liu, W.-F. Law, P.-L. Lau, J. Jiang and D. K. P. Ng, *Tetrahedron*, 1997, 53, 9087−9096.
30. W. Freyer, H. Stiel, K. Teuchner and D. Leupold, *J. Photochem. Photobiol*., 1994, 80, 161−167.
31. M. Hanack, G. Renz, J. Straehle and S. Schmid, *J. Org. Chem*., 1991, 56, 3501−3509.
32. W. Freyer, S. Mueller, K. Teuchner, *J. Photochem. Photobiol*., 2004, 163, 231−240.
33. T. Furuyama, Y. Ogura, K. Yoza and *N.* Kobayashi, *Angew. Chem*., 2012, 51, 11110−11114.

34. O. Matsushita, V. M. Derkacheva, A. Muranaka, S. Shimizu, M. Uchiyama, E. A.Luk'yanets and N. Kobayashi, *J. Am. Chem. Soc*., 2012, 134, 3411−3418.
35. M. S. Rodríguez-Morgade, B. Cabezoń, S. Esperanza and T. Torres, *Chem. -Eur. J*., 2001, 7, 2407−2413.
36. T. J. Marks and D. R. Stojakovic, *J. Am. Chem. Soc*., 1978, 100, 1695−1705.
37. V. W. Day, T. J. Marks and A. W. Wachter, *J. Am. Chem. Soc*., 1975, 97, 4519−4527.
38. J. Chen, Q. Gan, S. Li, F. Gong, Q. Wang, Z. Yang, S. Wang, H. Xu, J. S. Ma and G. Yang, *J. Photochem. Photobiol*., 2009, 207, 58–65.
39. X. -F. Zhang and Q. Xi, *Carbon*, 2011, 49, 3842–3850.
40. X. -F. Zhang and H. W. Zheng, *Inorganica. Chimica. Acta*., 2010, 363, 2259–2264.
41. D. A. C. Brownson and C. E. Banks, *Analyst*, 2010, 135, 2768–78.
42. D. Chen, L. Tang and J. Li, *Chem. Soc. Rev*., 2010, 39, 3157–80.
43. I. Carmichael and G. L. Hug, *J. Phys. Chem*., 1986, 15, 1.
44. S. R. Greeneld, W. A. Svec, M. R. Wasielewski, K. Hasharoni and H. Levanon, Springer-Verlag: Berlin, 1996; pp 81.
45. K. Hasharoni, H. Levanon, S. R. Greeneld, D. J. Gosztola, W. A. Svec and M. R. Wasielewski, *J. Am. Chem. Soc*., 1995, 117, 8055.
46. L. Dong, R. R. S. Gari, Z. Li, M. M. Craig and S. Hou, *Carbon*, 2010, 48, 781–7.
47. T. –H. Wei and A. A. Said, *IEEE Journal of Quantum Electronics*., 1990, 26, 4.
48. W. Wu, S. Zhang, Y. Li, J. Li, L. Liu and Y. Qin, *Macromolecules*, 2003, 36, 6286–8.

The effect of peripheral substituents attached to the phthalocyanines on the third order nonlinear optical properties of graphene oxide–zinc (II) phthalocyanine hybrids

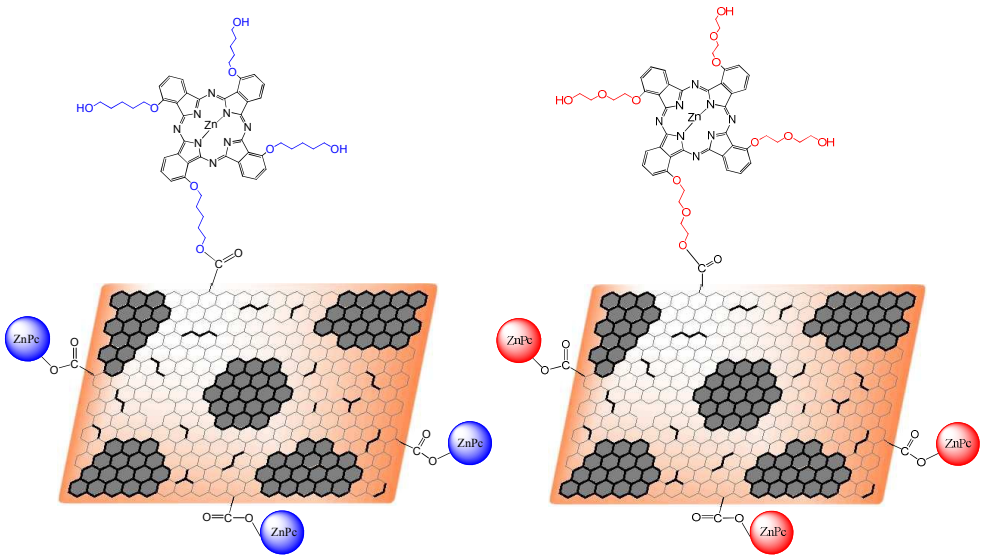

(GO-ZnPc(TD)$_4$) (A) (GO-ZnPc(DG)$_4$) (B)

SP^3 C-matrix (Grey-parts) 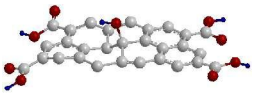 SP^2 C-cluster (black-parts) 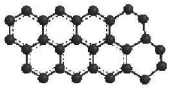

SP^2 C-congfiguration (black-lines) 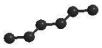

Both the two kinds of GO-ZnPc hybrid materials exhibit transformation of the NLO response from SA to RSA with the input intensity of 0.326 J/cm^2, and the β value of GO-ZnPc(DG)$_4$ is larger than that of GO-ZnPc(TD)$_4$ because GO-ZnPc(DG)$_4$ possesses the peripheral substituents of ZnPc(DG)$_4$ molecues with the stronger electron-donating effect.